

# High-field 1/f noise in hBN-encapsulated graphene transistors :

## Supplementary Information

A. Schmitt,<sup>1,\*</sup> D. Mele,<sup>1,2</sup> M. Rosticher,<sup>1</sup> T. Taniguchi,<sup>3</sup> K. Watanabe,<sup>3</sup> C. Maestre,<sup>4</sup> C. Journet,<sup>4</sup> V. Garnier,<sup>5</sup> G. Fève,<sup>1</sup> J.M. Berroir,<sup>1</sup> C. Voisin,<sup>1</sup> B. Plaçais,<sup>1,†</sup> and E. Baudin<sup>1,‡</sup>

<sup>1</sup>*Laboratoire de Physique de l'Ecole normale supérieure,  
ENS, Université PSL, CNRS, Sorbonne Université,  
Université de Paris, 24 rue Lhomond, 75005 Paris, France*

<sup>2</sup>*Univ. Lille, CNRS, Centrale Lille,  
Univ. Polytechnique Hauts-de-France, Junia-ISEN,  
UMR 8520-IEMN, F-59000 Lille, France.*

<sup>3</sup>*Advanced Materials Laboratory, National Institute for  
Materials Science, Tsukuba, Ibaraki 305-0047, Japan*

<sup>4</sup>*Laboratoire des Multimatériaux et Interfaces, UMR CNRS 5615, Univ Lyon,  
Université Claude Bernard Lyon 1, F-69622 Villeurbanne, France*

<sup>5</sup>*Université de Lyon, MATEIS, UMR CNRS 5510,  
INSA-Lyon, F-69621 Villeurbanne cedex, France*

### Abstract

This Supplementary Information contains a Table summarizing the geometrical and electrical parameters of the ten hBN-encapsulated graphene transistors series, as well as a description of the measurement setup. It presents a detailed description of the two-fluid flicker noise analysis. It is augmented by three figures detailing the DC transport (Fig.SI-4), velocity flicker noise (Fig.SI-5), and noise thermometry (Fig.SI-6) of 6 representative transistors discussed in the main text.

Sample name	Gate	hBN grade	L $\mu m$	W $\mu m$	$t_{hBN}$ nm	$R_c$ $\Omega$	$\mu(0)$ m <sup>2</sup> /Vs	$v_{sat}$ 10 <sup>6</sup> m/s	$\sigma_Z$ mS	A nm <sup>2</sup>	$E_\Lambda$ V/mm	dP/dT <sub>N</sub> MW/Km <sup>2</sup>
<b>Lyon1</b>	Au	PDC	9	9	142	250	<b>4</b>	0.82	0.1	0.64	67	0.068
<b>Lyon2</b>	Au	PDC	5	5	142	80	<b>8.5</b>	0.60	0.45	0.54	99	0.402
<b>InOut1</b>	Au	HPHT	12.5	17.5	164	71	<b>6</b>	0.33	0.40	0.57	48	0.373
<b>InOut2</b>	Au	HPHT	20	8.5	118	300	<b>11</b>	0.46	0.55	0.22	94	0.128
<b>GrS5</b>	Graphite	HPHT	3.8	4	98	100	<b>8</b>	0.48	0.60	0.36	56	0.461
<b>AuS3</b>	Au	HPHT	11.1	11.4	90	95	<b>15</b>	0.42	0.40	0.54	57	0.258
<b>Goyave2</b>	Au	HPHT	9	13	84	89	<b>2</b>	0.22	0.40	0.23	86	0.585
<b>Flicker162</b>	Au	HPHT	7.1	7.5	150	95	<b>14.5</b>	0.58	1.05	0.18	81	0.952
<b>Largevin2</b>	Si/SiO <sub>2</sub>	HPHT	5.4	25.4	59	40	<b>6</b>	0.36	0.25	0.61	89	0.452
<b>Coolox</b>	Si/AlO <sub>x</sub>	HPHT	5.3	5.8	86	140	<b>2</b>	0.38	0.27	0.26	140	0.262

TABLE SI-1: Geometrical and electrical properties of the 10 devices series. The first 6 devices are analyzed in Fig.3 of the main text. Basic properties include the nature of the gate electrode (Au or Graphite bottom gating, or back-gating with Si/SiO<sub>2</sub> or Si/AlO<sub>x</sub>) and the origin of the hBN dielectric, the channel length  $L$ , width  $W$ , hBN dielectric thickness  $t_{hBN}$ , and contact resistance  $R_c$ . We have used two hBN grades: the high-pressure high-temperature (HPHT) from NIMS and the polymer-derived ceramic (PDC) from Lyon. The mobility  $\mu(0)$ , saturation velocity  $v_{sat}$  and Zener interband conductivity  $\sigma_Z$  are extracted from DC measurements using Eq.(1) of the main text. The next two columns contain the two flicker parameters  $A$  and  $E_\Lambda$  deduced from the two-fluid flicker analysis (see Fig.3 of the main text), which are discussed in the main text. The last column contains the values of the thermal resistance to the hBN substrate  $dT_N/dP$  in the Zener interband regime, extracted from thermal noise measurements.

## I. A DETAILED PRESENTATION OF THE TWO-FLUID MODEL

This section aims at introducing in a detailed manner the two-fluid formula used in the main text for flicker noise analysis. The procedure is depicted in Fig.SI-2, taking the sample GrS5 as an example.

Let us start from the generalized Hooge formula for current noise  $S_I$  in the velocity saturation

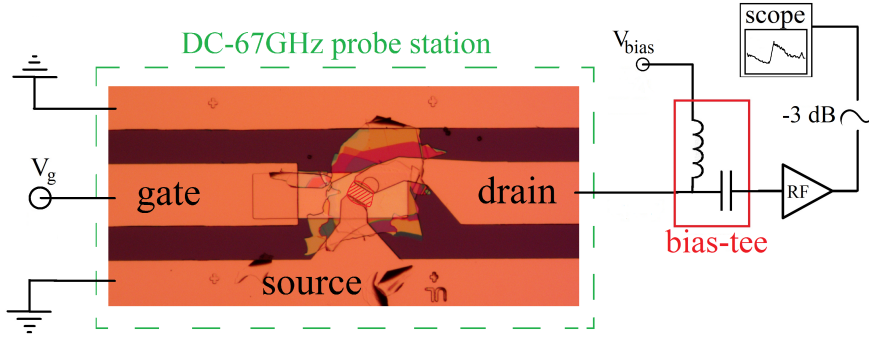


FIG. SI-1: Measurement setup for the probe-station characterization of DC transport, flicker and thermal noise in a high-mobility graphene transistor.

regime, introduced in Section III of the main text :

$$S_I(V) = (GV)^2 \frac{A}{LWf} \quad (1)$$

or equivalently for the current density noise-electric field  $S_J - E$  relation :

$$S_J(E) = (\sigma E)^2 \frac{A}{LWf} \quad (2)$$

where  $G = \partial I / \partial V$  is the differential conductance and  $\sigma$  the differential conductivity, and  $A$  is the flicker noise amplitude introduced earlier in graphene. Based on this formula, we introduce an interband contribution that is completely analogue, except that we assign to this interband term an exponential high-bias cutoff voltage  $V_\Lambda$  following the experimental observation in Figure 1d-Inset of the main text :

$$S_I(V) = (G_{sat}V)^2 \frac{A}{LWf} + (G_Z V)^2 \frac{B}{LWf} e^{-V/V_\Lambda} \quad (3)$$

or equivalently for the current density noise-electric field  $S_J - E$  relation :

$$S_J(E) = (\sigma_{sat}E)^2 \frac{A}{LWf} + (\sigma_Z E)^2 \frac{B}{LWf} e^{-E/E_\Lambda} \quad (4)$$

with  $B$  the amplitude for the interband term, and  $E_\Lambda = V_\Lambda / L$  the cutoff electric field. Note that the Zener conductance  $G_Z$  substitutes the saturation conductance  $G_{sat}$  in the interband term. Note also that we disregard here Pauli-blocking of Zener tunneling, which occurs below a doping-dependent electric field  $E_Z \lesssim E_{sat}$ , in a low bias regime where it leads to negligible conductivity corrections as  $\sigma_Z \ll ne\mu(0) \gtrsim 10$  mS. In this expression,  $G_{sat} = (W/L)\sigma_{sat} = (W/L)ne \frac{\mu(0)}{(1+V/V_{sat})^2}$  and  $G_Z$  are fully determined from the fits of the DC

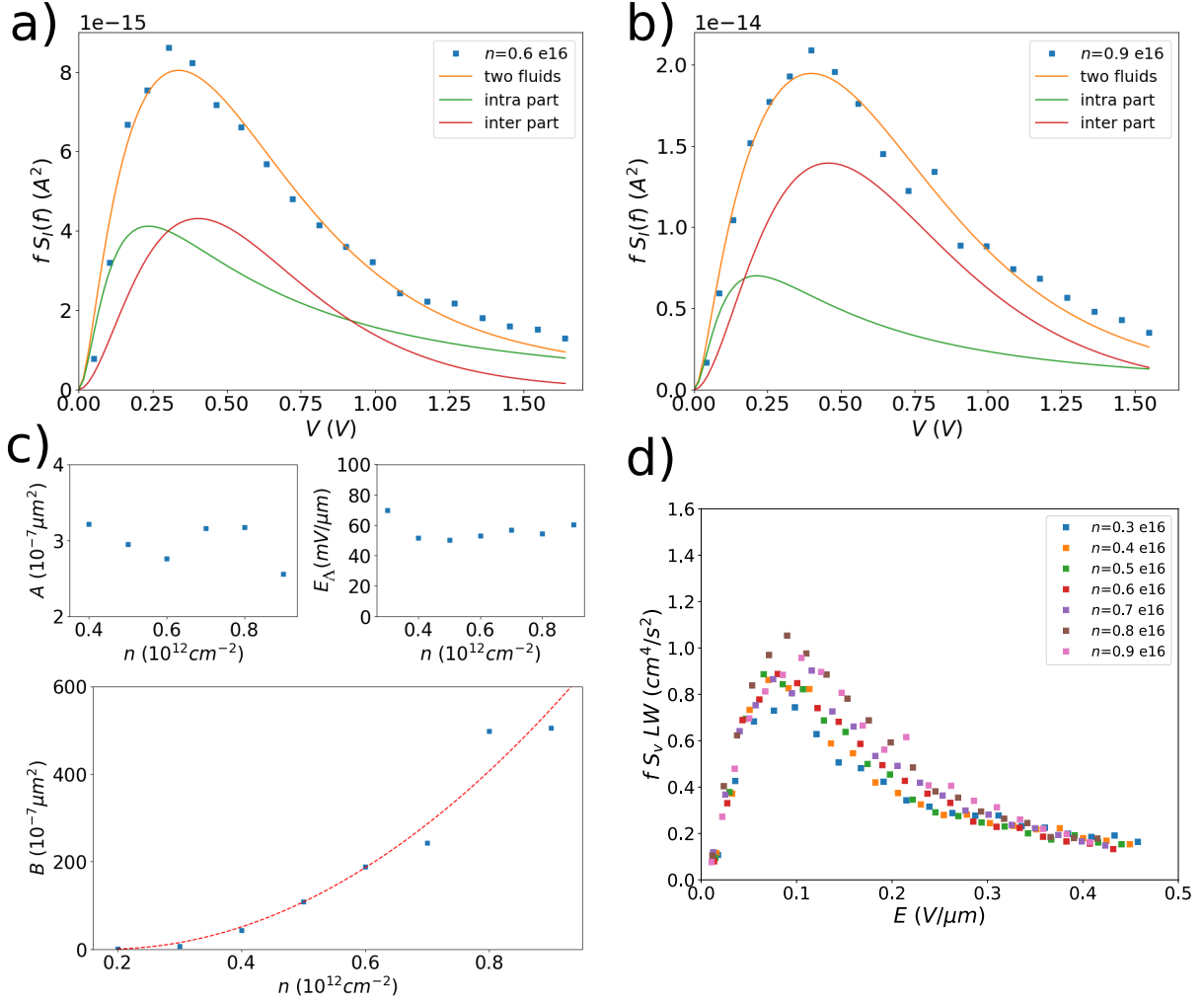


FIG. SI-2: Towards the two-fluid model, illustrated on the sample GrS5. Panels a) and b) show fits of the current noise  $S_I$  using Eq.(3) at density  $n = 0.6 \times 10^{12} \text{ cm}^{-2}$  and  $n = 0.9 \times 10^{12} \text{ cm}^{-2}$  respectively. c) Doping dependence of the three fitting parameters  $A$ ,  $B$  and  $E_\Lambda$ : while  $A$  and  $E_\Lambda$  appear doping-independent,  $B$  is hundred times larger and  $\propto n^2$  as illustrated by the red dotted-line fit. The joint  $G_{sat} \propto n$  and  $B \propto n^2$  dependencies in Eq.(3) lead to a velocity-noise scaling, as illustrated in panel d).

differential conductance described in Fig.SI-3, so that we are left with three fit parameters :  $A$ ,  $B$  and  $V_\Lambda$  (or  $E_\Lambda$ ). It is important to notice that the  $e^{-V/V_\Lambda}$  term is essential to avoid a divergence  $S_I \propto (G_Z V)^2$  at large bias due to the non-vanishing Zener conductance  $G_Z$ .

In a first step we perform fits of the current noise  $S_I$  using Eq.(3) for different values of doping (see panels a and b of Fig SI-2, for doping  $n = 0.6 \times 10^{12} \text{ cm}^{-2}$  and  $n = 0.9 \times 10^{12} \text{ cm}^{-2}$  respectively) and get perfect agreement. We represent the doping dependence of the fitting

parameters in Fig.SI-2c, and find  $A(n) \simeq \text{Cst.} \simeq 3 \cdot 10^{-7} \mu\text{m}^2$ ,  $E_\Lambda(n) \simeq \text{Cst.} \simeq 60 \text{ mV}/\mu\text{m}$ , and  $B(n) \propto n^2$ , as highlighted by the fit (red dotted line in panel c). Already at this point we report on the general trend that  $B \sim 100A$ .

Considering that both  $\sigma_{sat}^2 \propto n^2$  and  $B \propto n^2$ , the current noise  $S_J$  reduces to a doping-independent velocity flicker noise  $S_v = S_J \frac{1}{n^2 e^2}$ , that can be cast in the formula :

$$fS_v LW = A [\mu_{sat}(E)E]^2 + B \frac{n_\Delta^2}{n^2} [\mu_Z E]^2 e^{-E/E_\Lambda} \quad , \quad (5)$$

where the intraband mobility  $\mu_{sat}(E) = \frac{\mu(0)}{(1+E/E_{sat})^2}$ . A Zener mobility  $\mu_Z = \sigma_Z/(en_\Delta)$  is introduced as an apparent electron-hole pair mobility, associated to a density  $n_\Delta$  which is on the order of the out-of-equilibrium electron-hole pair density  $n_{eh}$  induced by Zener tunneling and hyperbolic cooling [1]. Velocity-noise scaling is quite robust, as illustrated in Fig.SI-2d for GrS5, and Fig.SI-5 for other devices. It corresponds to a ratio  $\frac{B}{A} \frac{n_\Delta^2}{n^2} \simeq \text{Cst.}$  independent of doping. At this point, as  $\mu_Z$  also depends on the electron-hole pair density  $n_\Delta$ , we need an additionnal Ansatz to quantify the ratio, which is achieved by setting  $A = \frac{2\alpha_0}{\pi n_\Delta}$ , following the IR bremsstrahlung interpretation of flicker noise. In the case of the sample GrS5, this yields an electron-hole pair density  $n_\Delta \simeq 1.5 \cdot 10^{12} \text{cm}^{-2}$  and an apparent interband mobility  $\mu_Z \simeq 0.25 \text{ m}^2/\text{Vs}$ . Most importantly, we can compute the ratio between the doping-independent amplitudes of the intraband and interband flicker noise contributions :

$$\frac{B}{A} \frac{n_\Delta^2}{n^2} \sim \frac{\pi\alpha_g}{2\alpha_0} = 150 \quad (6)$$

where  $\alpha_g = e^2/4\pi\epsilon_0\epsilon_{hBN}\hbar v_F \simeq 0.70$  the fine-structure constant for hBN-encapsulated graphene, introduced in the main text. This two-orders-of-magnitude larger amplitude for the interband contribution constitutes the main result of the three-parameter analysis. It is observed consistently on all the devices (we obtain  $\frac{B}{A} \frac{n_\Delta^2}{n^2} \in [30 - 800]$  depending on the device, with an average value  $\sim 150$ ) and justifies using a more robust two-parameter fit for the following two-fluid model that is used in the main text :

$$fS_v LW = A [\mu_{sat}(E)E]^2 + \frac{\pi\alpha_g}{2\alpha_0} A [\mu_Z E]^2 e^{-E/E_\Lambda} \quad (7)$$

where we have set for definiteness  $\frac{B}{A} \frac{n_\Delta^2}{n^2} = \frac{\pi\alpha_g}{2\alpha_0}$ , using  $A$  (or  $n_\Delta$ ) and  $E_\Lambda$  as the two remaining fit parameters (we keep relying on the same Ansatz  $A = 2\alpha_0/\pi n_\Delta$ , so that the value of  $A$  determines the value of  $\mu_Z = [\pi\sigma_Z/2e\alpha_0]A$ ).

Introducing a characteristic Zener velocity  $v_Z = \mu_Z E_\Lambda \simeq 0.015 v_F$ , we can cast the velocity-noise in the explicit formula used in the main text :

$$fS_v LW = Av_{sat}^2 \left[ \frac{E/E_{sat}}{(1 + E/E_{sat})^2} \right]^2 + \frac{\pi\alpha_g}{2\alpha_0} Av_Z^2 \left[ \frac{E}{E_\Lambda} e^{-E/2E_\Lambda} \right]^2 \quad (8)$$

that introduces the dimensionless field dependencies (terms into brackets) as well as the absolute scales  $Av_{sat}^2$  and  $\frac{\pi\alpha_g}{2\alpha_0} Av_Z^2$  of intra- and inter-band flicker noise. In the relative weight of the two contributions to noise, the imbalance  $v_Z \lesssim 0.05 v_{sat}$  is partly compensated by the large ratio  $\frac{\alpha_g}{\alpha_0} \sim 100$  between inter- and intra-band light-matter coupling constants. The values of  $A$  and  $v_Z^2$  of the different samples are displayed in panels a) and b) of the Figure 4 of the main text.

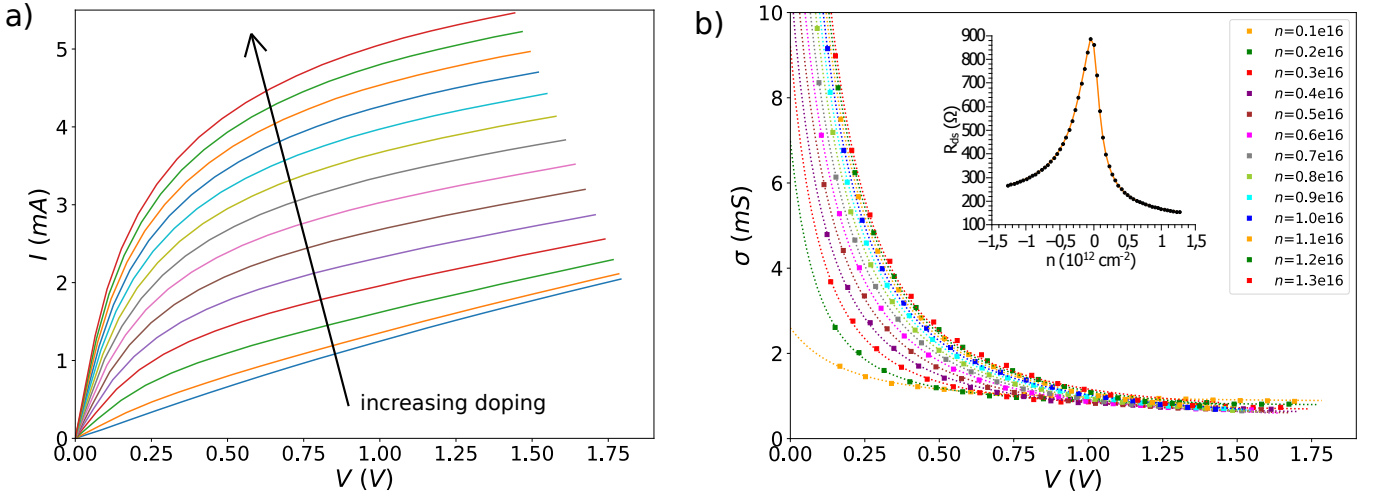


FIG. SI-3: DC transport analysis in the representative sample GrS5. a) Current-voltage curves measured at doping  $n = [0 - 1.3] 10^{12} \text{ cm}^{-2}$ . b) Differential conductivity  $\sigma = \frac{L}{W} \frac{\partial I}{\partial V}$  plotted as function of bias voltage  $V$ . The dotted lines correspond to fits using the formula  $\sigma(V) = ne \frac{\mu(0)}{(1+V/V_{sat})^2} + \sigma_Z$  from the main text and allow to extract the values of mobility  $\mu(0)$ , saturation voltage  $V_{sat}$  and Zener conductivity  $\sigma_Z$ . Note that  $\mu(0)$  agrees with standard mobility  $\mu$  deduced from the low-bias  $G(V_g)$  dependence. Errors in the determination of the fitted parameters are estimated to be  $\lesssim 1\%$ . Inset: zero-bias resistance versus doping. Associated values of mobility and contact resistance appear in Table SI-1, with a residual carrier density at neutrality  $n_0 \lesssim 7.10^{10} \text{ cm}^{-2}$ .

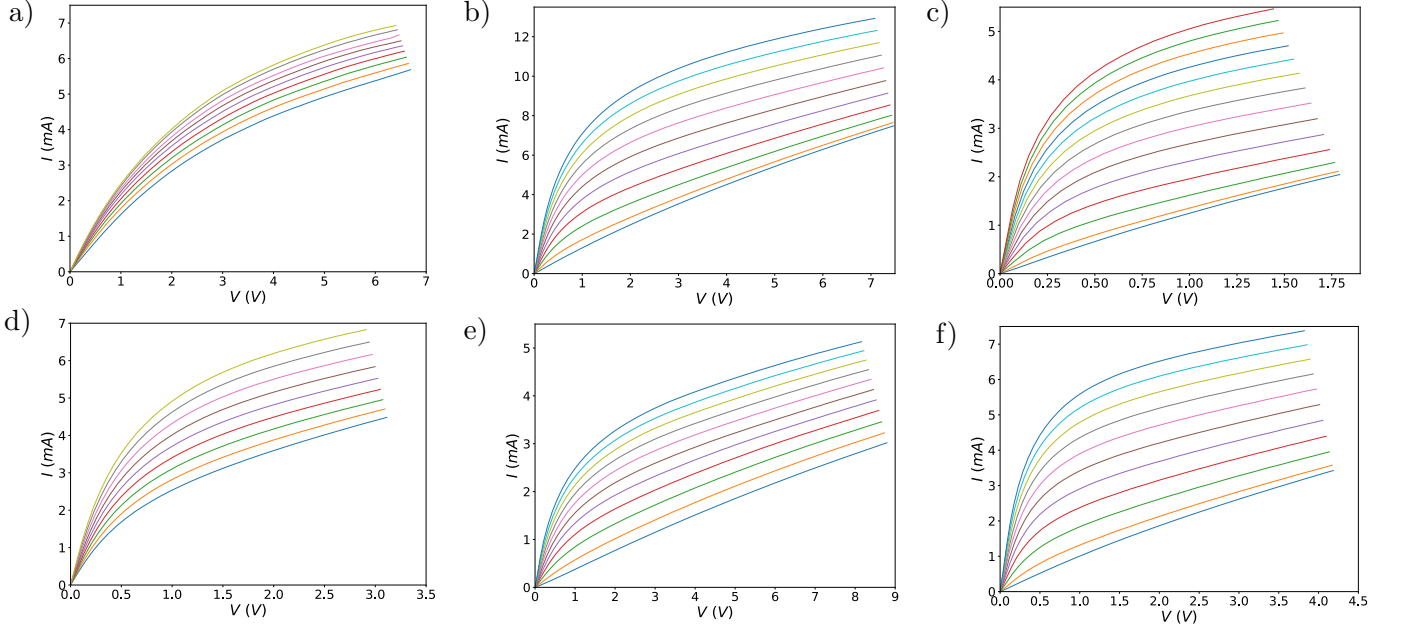


FIG. SI-4: Room temperature current voltage  $I(V)$  characteristics of 6 typical high-mobility graphene transistors : Lyon1 (a), InOut1 (b), GrS5 (c), Lyon2 (d), InOut2 (e), AuS3 (f). Their geometrical and electrical parameters are described in Table SI-1. The voltage drop across the contact resistance has been subtracted to access the local electric field  $E = V/L$  where  $L$  is the channel length. Main differences lie in the mobility ranging from  $\mu = 4 \text{ m}^2/\text{Vs}$  for Lyon1 (panel a) to  $\mu = 15 \text{ m}^2/\text{Vs}$  for AuS3 (panel f), and the Zener conductivity ranging from  $\sigma_Z = 0.1 \text{ mS}$  for Lyon1 (panel a) to  $\sigma_Z = 0.5 \text{ mS}$  for GrS5 (panel c).

---

\* Electronic address: aurelien.schmitt@phys.ens.fr

† Electronic address: bernard.placais@phys.ens.fr

‡ Electronic address: emmanuel.baudin@phys.ens.fr

<sup>1</sup> W. Yang, S. Berthou, X. Lu, Q. Wilmart, A. Denis, M. Rosticher, T. Taniguchi, K. Watanabe, G. Fève, J.M. Berroir, G. Zhang, C. Voisin, E. Baudin, B. Plaçais, *Nature Nanotechnol.* **13**, 47 (2018). *A graphene Zener-Klein transistor cooled by a hyperbolic substrate*

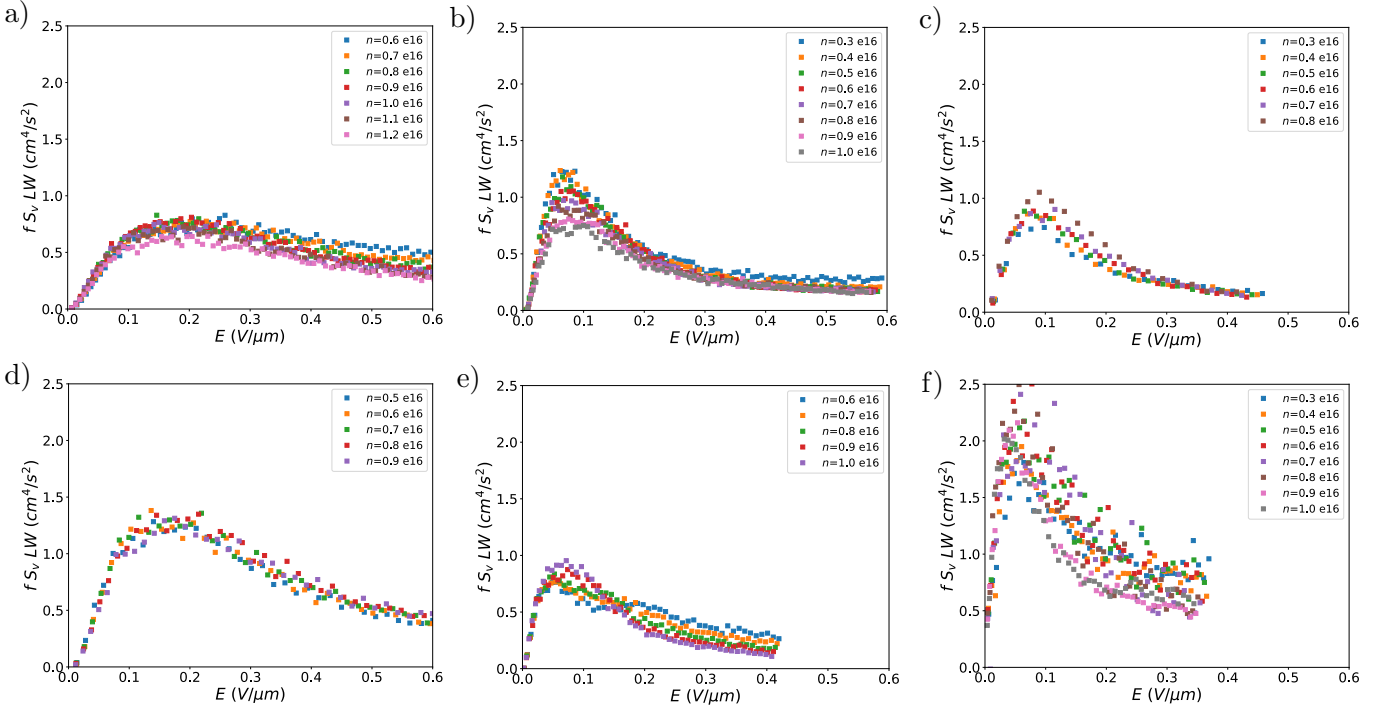


FIG. SI-5: Intensive velocity flicker noise  $fS_v LW(E)$  as function of electric field  $E = V/L$  for 6 typical high-mobility graphene transistors : Lyon1 (a), InOut1 (b), GrS5 (c), Lyon2 (d), InOut2 (e), AuS3 (f). Their geometrical and electrical parameters are described in Table SI-1. Velocity noise  $S_v = S_I/n^2 e^2 W^2$  is deduced from the measured current noise  $S_I$  accounting for electrostatic doping  $n$  and sample width  $W$ . The figure illustrates the scaling property of the velocity flicker as discussed in the main text. Sample statistics reveal a rather universal velocity-flicker amplitude  $fS_v LW = 1-2 \text{ cm}^4/\text{s}^2$ , and significant variability in the electric-field dependence.

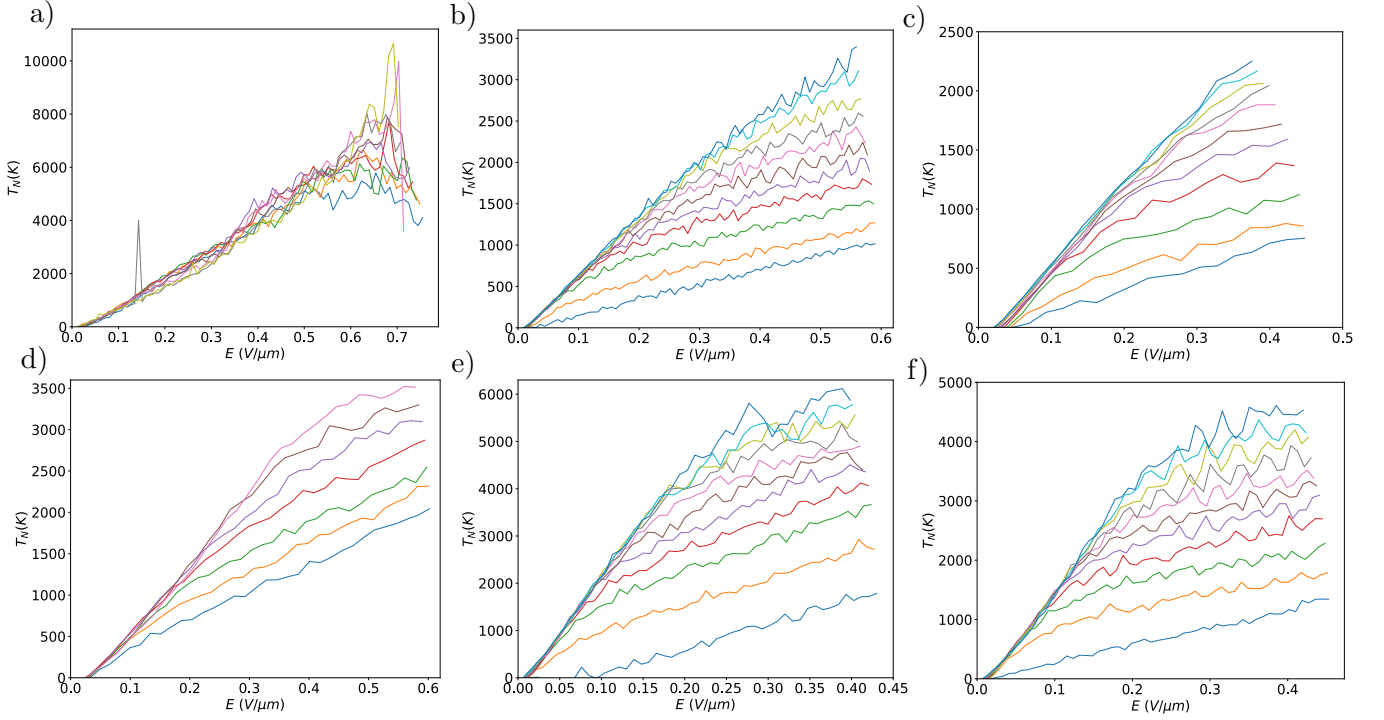


FIG. SI-6: Noise temperature  $T_N(E)$  as function of electric field  $E$  for 6 typical high-mobility graphene transistors : Lyon1 (a), InOut1 (b), GrS5 (c), Lyon2 (d), InOut2 (e), AuS3 (f). Their geometrical and electrical parameters are described in Table SI-1.  $T_N(E)$  is deduced from the Johnson-Nyquist noise  $S_I = 4Gk_B T_N$ , measured in the flicker-free 1-10 GHz microwave band, taking the DC differential conductance  $G$  as a prefactor. It characterizes the cooling pathways at stake in increasing  $E$ : the in-plane heat conduction at low  $E$  which depends on mobility, and the radiative cooling by hyperbolic phonon polariton (HPhP) emission in the hBN substrate in the Zener regime at large  $E$ . Significant sample to sample variability is observed that reflects the sensitivity of hot-electron temperature to electronic mobility at low- $E$  and to the mobility of hBN-HPhPs at large- $E$  with a reduced HPhP cooling in the hBN-PDC-grade transistors Lyon1 (panel a) and Lyon2 (panel d), with respect to the hBN-HPhP-grade transistors (other panels).